Joint Pathology Center
Veterinary Pathology Services

WEDNESDAY SLIDE CONFERENCE 2012-2013

Conference 18

13 February 2013

CASE I: M09-03439/ 3429 (JPC 3139508).

Signalment: 4-year-old, female Anglo Nubian goats *(Capra aegagrus hircus)*.

History: Four out of twenty-five stud goats from a herd in Northern NSW died suddenly after displaying ataxia, tachycardia, dilated pupils, pyrexia (38.2C), head tilt and stargazing. The submitting clinician necropsied one animal, and found a "diffuse white pattern in the liver." No other changes were reported. The entire brain and sections of liver were submitted. There was a recent introduction of new hay.

1-1. Liver, goat: Centrilobular hemorrhage is prevalent at subgross inspection. (HE 40X)

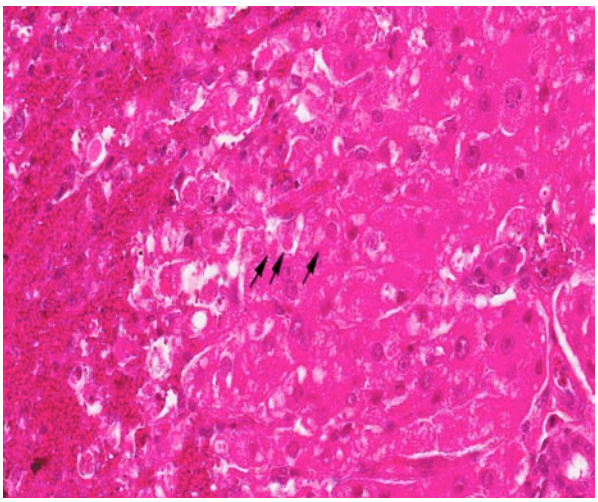

1-2. Liver, goat. A range of degenerative (cytoplasmic vacuolation, cytosegresome formation - arrows) and necrotic changes (individualized, rounded up, hypereosinophlic granular cytoplasm, and karyorrhexis) are present with remaining hepatocytes in centrilobular and midzonal areas. At left, hemorrhage obscures necrotic hepatocytes within the lobule's center. (HE 400X)

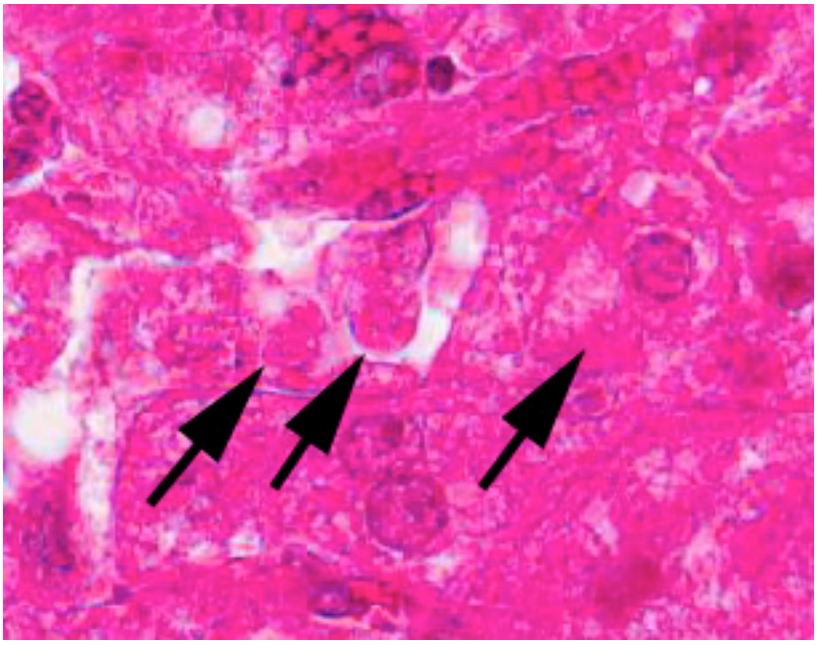

1-3. Liver goat: Cytosegresomes are autophagic vacuoles induced in hepatocytes by a wide range of sublethal insults. (HE 400X)

Histopathologic Description: There is extensive centrilobular necrosis with replacement hemorrhage. Hepatocytes at the margins of the necrotic zones contain multiple fine vacuoles. Occasional cytosegresomes are noted, and individualized, shrunken hepatocytes are scattered through the section. There is mild to focally moderate hepatocytic cellular size variation, with an increase in mitotic figures. Larger bile ducts are frequently lined by hyperplastic epithelium, and there are multiple zones with increased numbers of intraepithelial lymphocytes.

Contributor's Morphologic Diagnosis: 1. Hepatic necrosis, centrilobular, severe, coalescing, acute.
2. Mild biliary epithelial hyperplasia.

Contributor's Comment: The submitting veterinarian made a note that a number of potential poisonous plants were present in the fields, including a heavy growth of *Trema tomentosa* (formerly *Trema aspera*), more commonly known as poison peach.

Poison peach is a large leafy shrub or small tree distributed along Eastern and Northern Australia, extending into New Guinea. It grows mainly in moist open forest, and is considered a pioneer species – frequently becoming a dominant growth following deforestation. Cattle and sheep readily eat the leaves when access is given. In Australia, leaves and fine stems have been shown to be toxic to many livestock species - presumably due to the presence of a glycoside named "trematoxin," which acts as a hepatic toxin.[2] Death due to its ingestion has been reported in Australia in cattle, sheep, horses and camels. Experimentally, toxicity can be easily induced in rabbits and guinea pigs. The submitters have been unable to find any description of toxicity in the literature.

Its relative, *Trema micrantha*, is widely dispersed in Central and South America. It is also a pioneer species and is being considered as a prime candidate in replantings and restoration of degraded forest land. The tree contains toxins which induce a profound hypoglycaemia in rats, and some trials have been carried out touting this agent as an alternative treatment for diabetes mellitus in humans.[4] One reference (in Portuguese) was found citing toxicity in cattle[4] and experimentally in rabbits[6], both of which suggest pathological changes similar, if not identical, to those seen in *Trema tomentosa.* Toxicity in livestock induced by *T. micrantha* appears to be more prevalent in Brazil, explaining the tendency for more recent reports to be in the non-English literature.

The differential diagnosis for this histological pattern in ruminants should include the common suspects of microcystin (blue green algae), green cestrum (*Cestrum* spp.), and noogoora burr (*Xanthium pungens*). The chinaberry or white cedar tree (*Melia azedarach)* contains four teranortriterpenes (meliatoxins A1, A2, B1 and B2), which can variably lead to massive central necrosis; however, these changes are less uniform that those noted above.[3]

JPC Diagnosis: Liver, centrilobular hepatocytes: Degeneration and necrosis, diffuse, acute, with marked hemorrhage.

Conference Comment: We have seen several examples of various types of hepatic toxicity in this year's conferences. The liver is a common site of toxic injury, as it is exposed to numerous ingested substances through the portal blood. There are six

categories of hepatotoxic liver injury, based on the cellular targets of the injurious substances. The most common mechanism involves biotransformation by the cytochrome p-450 system that results in toxic metabolites. Because cytochrome p-450 is most abundant in the centrilobular areas, the result is centrilobular necrosis, as in this case of poison peach toxicity. The second category is characterized by the formation of adducts between drugs and cellular enzymes, other proteins or nucleic acids that act as antigens that, once recognized by the immune system, trigger an inflammatory response against the hepatocytes or biliary epithelium that contain them. A third category involves toxins (such as retained or excess bile acids) that trigger apoptosis of hepatocytes either by direct stimulation of pro-apoptotic pathways or immune mediated events that release TNF-alpha or activate Fas apoptosis pathways. The fourth category of hepatic toxicity is caused by the disruption of calcium homeostasis by cell membrane damage or disruption of enzymes responsible for maintaining intracellular calcium concentrations. This disruption leads to increased intracellular calcium, which activates proteases that damage actin filaments such that further damage to cell membranes results. The fifth category of toxic injury to the liver manifests as intracellular cholestasis, as the pumps that secrete bile into the canaliculi can be disrupted by certain chemicals (such as estrogen, erythromycin) or by hepatocellular injury that affects the canalicular pumps or actin filaments around the canaliculi. Finally, the sixth category of hepatic toxicity is hepatocellular injury and death due to mitochondrial damage. Mitochondrial damage can result in hepatocyte injury, apoptosis or necrosis via several mechanism, including release of reactive oxygen species, decreased ATP, and decreased beta-oxidation of lipids leading to microvesicular steatosis (lipid accumulation), or release of cytochrome-c which triggers apoptosis.[1]

The distribution of hepatocellular injury reflects the mechanism and cellular targets of the toxin. Toxins that require bioactivation by cytochrome p-450 metabolism result in centrilobular or paracentral (periacinar) degeneration and necrosis. Midzonal degeneration and necrosis are uncommon lesions, but have been reported with aflotaxicosis in pigs and horses. Periportal hepatocellular injury occurs with cholestasis-related injury or toxins that do not require cytochrome p-450 metabolism (e.g. white phosphorous).[1] Other mechanisms, such as toxins that cause mitochondrial or cellular membrane damage, may result in a more diffuse distribution of injury.

Contributing Institution: Veterinary Laboratory
Department of Primary Industries
New South Wales
Woodbridge Rd
Menangle, NSW 2568
Australia
www.dpi.nsw.gov.au

References:

1. Cullen JM, Brown DL. Hepatobiliary system and exocrine pancreas. In: McGavin MD, Zachary JF, eds. *Pathologic Basis of Veterinary Disease*. 5th ed. St. Louis, MO: Elsevier Mosby; 2012:437-439.
2. Oelrichs PB. Isolation and purification of trematoxin from Trema aspera. *Phytochemistry*. 1968:7:1691-1693.
3. Oelrichs PB, Hill MW, Vallely PJ, et al. Toxic tetranortriterpenes of the fruit of Melia azedarach. *Phytochemistry*. 1983;22:531-534.
4. Schoenfelder T, Cirimbelli TM, Citadini-Zanette V. Acute effect of Trema micrantha (Ulmaceae) on serum glucose levels in normal and diabetic rats. *Journal of Ethnopharmacology*. 2006;107:456-459.
5. Traverso SD, Correa AMR, Schmitz M, et al. Experimental poisoning by Trema micrantha (Ulmaceae) in cattle. *Pesquisa Veterinaria Brasileira*. 2004;24:211-216.
6. Traverso SD, Driemeier D. Experimental Trema micrantha (Ulmaceae) poisoning in rabbits. *Veterinary and Human Toxicology*. 2000;42:301-302.

CASE II: D1395000028 (JPC 3174953).

Signalment: Nine-week-old, male, Sprague-Dawley rat *(Rattus norvegicus)*.

History: This rat was administered 400 mg/kg gentamicin subcutaneously once daily on days 1, 2 and 3 to induce renal tubular injury. Serum and urine were collected on day 4 for urinalysis and serum chemistry analysis; pertinent data is listed in the tables below. The rat was euthanized and necropsied 48 hours after administration of the last dose of gentamicin.

Gross Pathologic Findings: Kidneys were bilaterally pale on gross examination.

Laboratory Results:

Serum chemistry	**Normal**	**Day 4**	**Day 5**
BUN, mg/dL	7 - 27	30	103
Creatinine, mg/dL	0.4 – 1.8	0.8	3.0
Phosphorus, mg/dL	2.1 – 6.3	9.5	13.0
Urinalysis		**Day 4**	**Day 5**
Specific gravity		1.010	1.016
Protein, mg/dL		<100	300-500

Histopathologic Description: The slide contains one section of kidney. There is widespread degeneration and necrosis of the proximal convoluted tubules of the cortex. Frequently, the cytoplasm of the degenerate and necrotic cells contains discrete, variably sized, hyaline granules to globules (hyaline droplets). There are rare attempts at epithelial restitution characterized by more squamous-appearing epithelial cells which have spread to cover denuded basement membrane. Necrotic epithelial cells are hypereosinophilic with pyknotic or karyolytic nuclei (coagulation necrosis) and are individualized and desquamating into the tubular lumen. There is often complete dissolution of necrotic epithelial cells into fine, eosinophilic granular cellular debris which fills the tubular lumen. The interstitium is multifocally expanded by scant clear space (interstitial edema). There is widespread proliferation of interstitial cells in the cortex predominantly surrounding glomeruli but also seen scattered between tubules. Admixed with the proliferating interstitial cells are low numbers of lymphocytes and histiocytes. Distal convoluted tubules in the cortex are more apparent with large vesicular nuclei and increased cytoplasmic basophilia. Increased numbers of mitotic figures, large vesicular nuclei and cytoplasmic basophilia are also seen in tubular epithelial cells within the outer and inner medullary stripe. Many tubules of the outer stripe are lined by epithelial cells which have intense hyaline cytoplasmic droplet formation. Scattered tubules within the outer and inner medullary stripe and papilla contain proteinaceous fluid (hyaline casts), granular eosinophilic debris, desquamated necrotic cells or cellular debris (cellular casts) and/or deeply basophilic to purple granular material (mineral).

Contributor's Morphologic Diagnosis: 1. Acute diffuse degeneration and necrosis of the cortical proximal tubules with cytoplasmic hyaline droplet formation.
2. Cortical interstitial cell proliferation with mild lymphohistiocytic interstitial nephritis.

Contributor's Comment: Gentamicin is almost exclusively filtered by the glomerulus and excreted unchanged by the kidney. Nephrotoxicity results from reabsorption and accumulation of gentamicin in proximal convoluted tubule (PCT) epithelial cells.[8] Gentamicin is a cationic molecule that binds anionic phospholipids in the brush border of the PCT epithelial cells with endocytotic uptake leading to its lysosomal sequestration. Binding of gentamicin to the anionic phospholipid membranes impairs the hydrolysis of phosphatidylcholine in the bilayer by sphingomyelinase and other phospholipases and results in lysosomal phospholipidosis.[7] There is an increase in size and number of phagolysosomes, which are ultrastructurally called myeloid bodies. Myeloid bodies are membrane bound vesicles characterized internally by electron-dense, concentrically whorled membranes (myelin figures) and membrane fragments, and may contain altered cellular organelles including mitochondria. There is also loss of microvilli and cytoplasmic blebbing of the apical PCT.[3]

There are several hypotheses as to the mechanism of PCT cell necrosis in gentamicin-induced nephrotoxicity. Gentamicin changes lysosomal membrane permeability which may result in lysosomal enzyme leakage and necrosis.[9] There are several examples of PCT lysosomal overload resulting in toxicity such as in the unique male rat α2u-globulin nephropathy, Bence-Jones nephropathy and nitrilotriacetic acid nephrotoxicity. It has been suggested that gentamicin is toxic

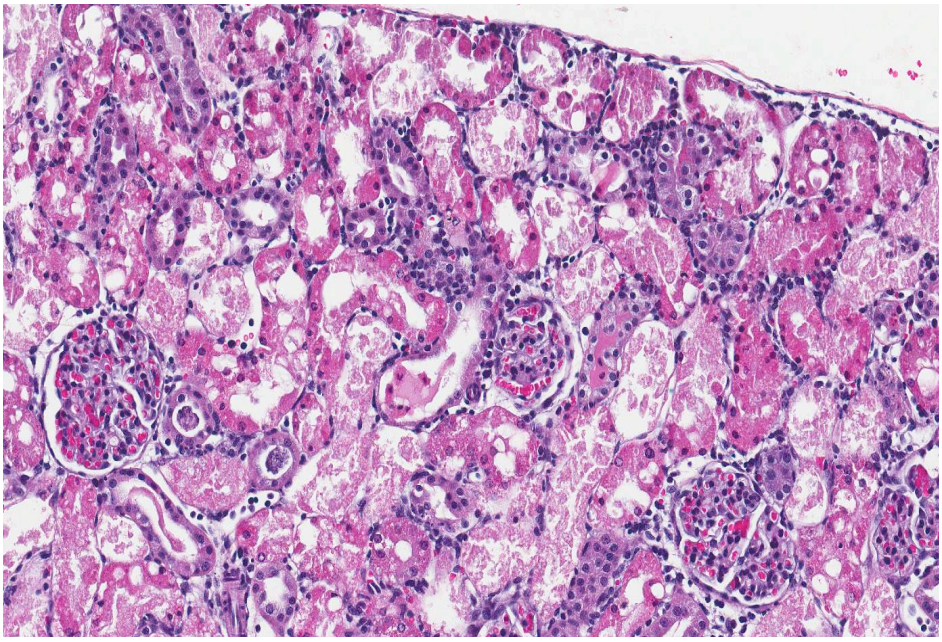

2-1. Kidney, Sprague-Dawley rat: Throughout the cortex, proximal convoluted tubular epithelium exhibits extensive degeneration and necrosis. (HE 60X)

through non-lysosomal targets including disruption of ion transport and enzyme release at the apical and basolateral membranes.[9] Recent studies have indicated free radicals are important mediators of damage in gentamicin nephrotoxicity. Gentamicin has been shown to enhance the generation of superoxide anion and hydrogen peroxide by mitochondria. Gentamicin has also been shown to lead to the release of iron from renal cortical mitochondria and to enhance generation of hydroxyl radicals which are produced by the superoxide anion and hydrogen peroxide in the presence of a metal catalyst, in this case iron. Free radical scavengers and metal chelators have been shown to ameliorate gentamicin-induced renal injury.[1]

On gross examination the kidneys may be pale and enlarged. Microscopically, acute tubular necrosis is restricted to the S1 and S2 segments (pars convoluta) of the PCT, though hyaline droplets are prominent throughout all segments of the proximal tubule.[9] Clinically gentamicin toxicity results in the inability to concentrate urine, polyuria, glucosuria, proteinuria, phospholipiduria and increased serum BUN and creatinine.[8] Dysfunction of the PCT results in decreased uptake of glucose, organic bases and low molecular weight protein resulting in their excretion in the urine. Phospholipiduria results in phospholipid-rich myeloid bodies that are shed from the damaged microvillar surfaces of the PCT and can be seen in the urine sediment.[3]

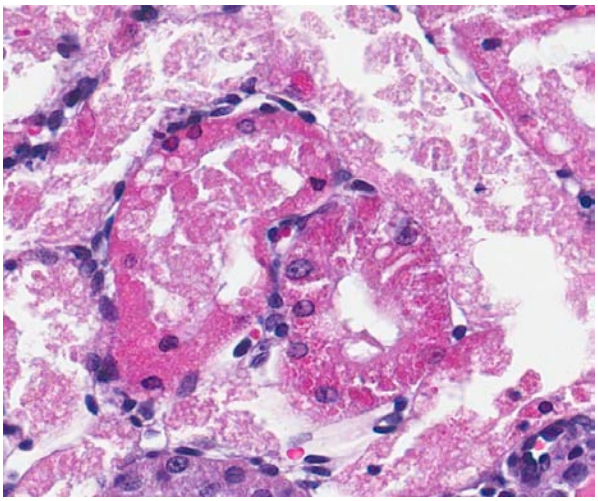

2-2. Kidney, Sprague-Dawley rat: Sublethal injury to proximal convoluted tubule epithelium by aminoglycosides often results in an accumulation of brightly eosinophilic lysosomes filled with phosphopids, as a result of the drug's antagonistic effect on cellular phospholipases. (HE 400X)

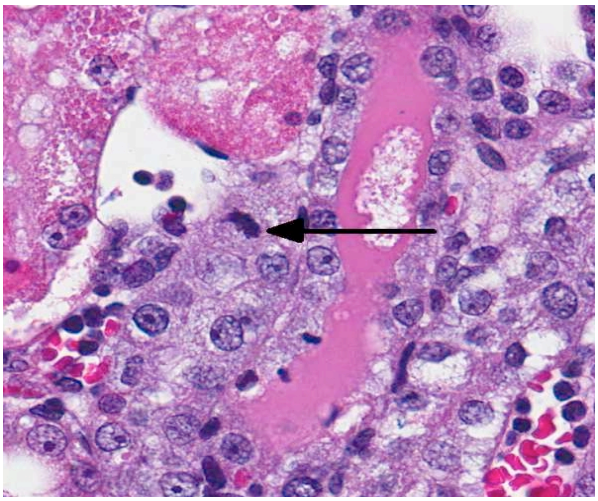

2-3. Kidney: Regenerating tubules exhibit cytoplasmic basophilia, enlarged nuclei with vesicular chromatin, and often, mitotic figures (arrow). (HE 400X)

Proximal tubule intracytoplasmic hyaline droplet formation may be associated with accumulation of α2u-globulin. This is a gender specific phenomenon and is only seen in mature male rats. These hyaline droplets represent an accumulation of secondary lysosomes containing α2u-globulin and/or albumin within the cytoplasm. Under toxicologic and pathologic conditions hyaline droplets may also consist of other proteins (e.g. histiocytic sarcoma associated hyaline droplets contain lysozyme).[6] Hyaline droplet formation is thought to occur through two mechanisms: increased endogenous protein production or interference with lysosomal enzyme-mediated hydrolysis occurring in the renal epithelial cell. It has been reported that lysosomal bodies in the PCT of rats autofluoresce[5]; the hyaline droplets in the PCT of this rat demonstrate this phenomenon. A Mallory's Heidenhain or chromotrope-aniline-blue stain is used to visualize the α2u-globulin component and PAS is used to demonstrate the albumin component of the hyaline droplets in this case.[4,5,7] As a highly exaggerated dose of gentamicin was used in this study to enable a rapid development of necrosis, specific evidence of phospholipidosis in H&E section are not apparent in this case. However, a Baker's stain in frozen section or a toluidine blue stain of plastic section could be anticipated to dramatize the phospholipidotic accumulations and debris.

Gentamicin nephrotoxicity can be reversible. Regeneration of PCT epithelium progresses even with continued dosing of gentamicin. It is thought that regenerating epithelium is more resistant to toxicity than mature PCT epithelium.[8] However, over chronic time frames in toxic exposures, even at doses that do not cause necrosis, increased cell turnover can be demonstrated and exacerbation of lesions of chronic progressive nephropathy may be the longer term consequence.

JPC Diagnosis: Kidney, proximal convoluted tubules: Degeneration, necrosis and regeneration, with abundant protein casts.

Conference Comment: The kidney is a major site of drug-induced injury, primarily because approximately one quarter of the cardiac output is delivered to the kidneys, where substances in the blood are filtered, biotransformed, and concentrated. Toxins or toxic metabolites can then result in renal cell damage and death in a variety of ways. Renal epithelial cells can be damaged directly, as often occurs in proximal convoluted tubules after intracellular biotransformation converts a drug to reactive metabolites. Alternatively, reactive metabolites can be generated in the tubular filtrate, causing renal tubular epithelial necrosis upon reabsorption. Some nephrotoxins cause vasoconstriction and ischemia-related cell death.[10]

Because of their unique mechanisms of toxicity, different drugs affect different specific segments of the nephron, which may assist in narrowing the differential diagnosis in a diagnostic setting. The proximal convoluted tubule is the most commonly-affected segment; numerous drugs cause injury here, including gentamicin, cyclosporine, and cisplatin. The distal tubules are damaged by cyclosporine, sulfadiazine, and amphotericin B, among others. The collecting duct is affected by amphotericin B and acyclovir, and the loop of Henle can be damaged by chronic exposure to analgesics. Glomerular damage can be caused by doxorubicin, gold and penicillamine.[2]

Conference participants discussed serum biomarkers of renal injury such as serum creatinine and blood urea nitrogen, which despite lacking sensitivity, are commonly used to detect renal damage, and are elevated in severe renal disease, as in this case. Serum creatinine, the standard biomarker for glomerular filtration rate, increases only after substantial injury, and is affected by both systemic production and tubular secretion of creatinine. Blood urea nitrogen is also used to measure renal function, but it can be affected by many factors, including urea production by the liver; in addition to being filtered by the glomerulus, it is also reabsorbed by other parts of the nephron.[2] For these reasons, recent research through the Predictive Safety Testing Consortium has been aimed at identifying second-generation biomarkers for acute kidney injury in both laboratory animal models and humans. The goal is to identify markers for early detection of renal injury as well as localization of the injury. Although none have yet shown sufficient specificity and sensitivity for clinical use, several markers have been proposed, including the following:[2]

- Kidney injury molecule-1 (KIM-1), interleukin-18 (IL-18), and fatty acid binding protein-liver type (L-FABP) which are increased with damage to proximal tubules
- Neutrophil gelatinase-associated lipocalin (NGAL) and clusterin, which are associated with damage to proximal and distal tubules

- Osteopontin, which is associated with damage to proximal tubules, loops of Henle and distal tubules
- Cystatin C, which is associated with damage to glomeruli and proximal tubules

Histopathology remains the gold standard for identifying renal injury; however, these or other biomarkers may prove to reliably detect kidney injury in both experimental animals and in a clinical setting.[2]

Contributing Institution: Millennium: The Takeda Oncology Company
35 Landsdowne Street
Cambridge, MA 02139
http://www.mlnm.com/

References:

1. Baliga R, Ueda N, Walker PD, Shah SV. Oxidant mechanisms in toxic acute renal failure. *Drug Metab Rev*. 1999;31:971-997.
2. Bonventre JV, Vaidya VS, Schmouder R, Feig P, Dieterle F. Next-generation biomarkers for detecting kidney toxicity. *Nat Biotechnol*. 2010;28:436-440.
3. Cheville N. *Ultrastructural Pathology: The Comparative Cellular Basis of Disease*. 2nd ed. Ames, Iowa: Wiley-Blackwell; 2009.
4. de Rijk EP, Ravesloot WT, Wijnands Y, van Esch E. A fast histochemical staining method to identify hyaline droplets in the rat kidney. *Toxicol Pathol*. 2003;31:462-464.
5. Hard GC. Some aids to histological recognition of hyaline droplet nephropathy in ninety-day toxicity studies. *Toxicol Pathol*. 2008;36:1014-1017.
6. Hard GC, Snowden RT. Hyaline droplet accumulation in rodent kidney proximal tubules: an association with histiocytic sarcoma. *Toxicol Pathol.* 1991;19:88-97.
7. Haschek WM, RC, Wallig WA. Handbook of Toxicologic Pathology, Two-Volume Set, 2 ed. San Diego, CA: Academic Press; 2002.
8. Maxie MG. *Jubb, Kennedy and Palmer's Pathology of Domestic Animals*. Philadelphia, PA: Elsevier Saunders; 2007.
9. Mingeot-Leclercq MP, Tulkens PM. Aminoglycosides: nephrotoxicity. Antimicrob Agents *Chemother*. 1999;43:1003-1012.
10. Newman SJ. The urinary system. In: McGavin MD, Zachary JF, eds. *Pathologic Basis of Veterinary Disease*. 5th ed. St. Louis, MO: Elsevier Mosby; 2012:602-603.

CASE III: 09/191 (JPC 3148216).

Signalment: Seven-year-old, male, German shepherd, *Canis familiaris*, dog.

History: At presentation to the clinic at the Norwegian School of Veterinary Science, the dog had a one-week history of anorexia, vomiting and diarrhea. Clinical examination showed below normal body condition, dehydration, listlessness and necrotic ulcers of oral mucosa.

Gross Pathologic Findings: Perianal skin was contaminated with dark feces. From mid-jejunum and aborally the intestinal content was dark. There was mineralization of pleura between ribs 2, 3 and 4, on vocal cords and subintimally in the pulmonary artery and vein. The endocardium of the left atrium was hyperemic and mildly rugous. The kidneys were moderately swollen with a moist cut surface and cortical pale radiating stripes.

Laboratory Results: Serum samples showed hyperkalemia, hypoglycemia and severely elevated creatinine (2900 µmol/L). Blood gas analysis showed severe metabolic acidosis (pH 7.1).

In serum collected on the day of presentation at the clinic ethylene glycol or glycolic acid was not detected. Fresh renal tissue collected at the time of necropsy showed presence of glycolic acid.

Histopathologic Description: Multifocally renal tubules are moderately dilated and commonly show a flattened attenuated epithelium. There is mild tubular epithelial hydropic degeneration and necrosis characterized by hypereosinophilic cytoplasm and pyknotic and karyorrhectic nuclei. Many proximal tubules show epithelial loss and contain dark, basophilic, birefringent material (von Kossa positive calcium deposits) filling the space delineated by intact tubular basement membranes. Some tubules contain hyaline or granular casts. The granular casts are characterized by eosinophilic granular material (cytoplasmic debris) and basophilic finely granular material (nuclear debris and calcium deposits). Some tubular epithelial cells show mitosis (regeneration). There is a moderate amount of intratubular sheaves and bundles of faintly yellow material showing birefringence in polarized light (crystals of calcium oxalate). Some tubular epithelial cells contain intracytoplasmic brown pigment (hemosiderin), and rarely intranuclear eosinophilic inclusions (incidental finding). Focally there is a mild interstitial infiltration of lymphocytes and fewer plasma cells. Bowman's space is focally moderately dilated, ands show sloughing of parietal epithelium.

Contributor's Morphologic Diagnosis: 1. Kidney: Tubular degeneration, necrosis and loss with intratubular calcium deposits and calcium oxalate crystals.
2. Kidney: Nephritis, interstitial, lymphoplasmacytic, multifocal, mild.

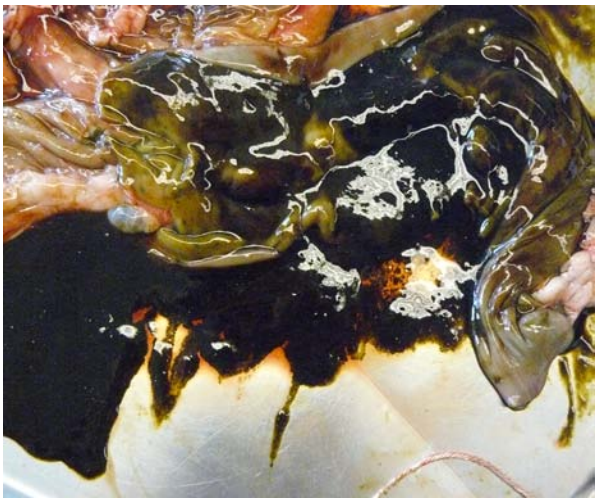

3-1. Intestine, dog: The jejunum and aboral GI tract contained dark contents. (Photo courtesy of the Norwegian School of Veterinary Science, Departments of Basic Sciences and Aquatic Medicine, POB 8146 Dep N-0033, Oslo, Norway; www.nvh.no)

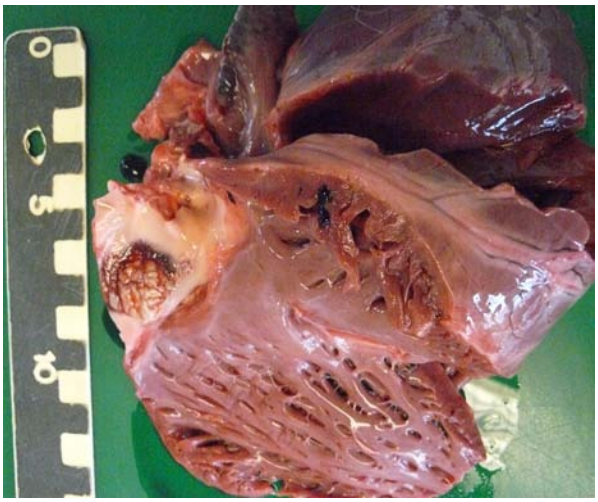

3-2. Heart, dog: There was mineralization subintimally in the pulmonary artery and vein. The endocardium of the left atrium was hyperemic and mildly rugose. (Photo courtesy of the Norwegian School of Veterinary Science, Departments of Basic Sciences and Aquatic Medicine, POB 8146 Dep N-0033, Oslo, Norway; www.nvh.no)

3-3. Kidney, dog: The kidneys were moderately swollen with a moist cut surface and cortical pale radiating stripes. (Photo courtesy of the Norwegian School of Veterinary Science, Departments of Basic Sciences and Aquatic Medicine, POB 8146 Dep N-0033, Oslo, Norway; www.nvh.no)

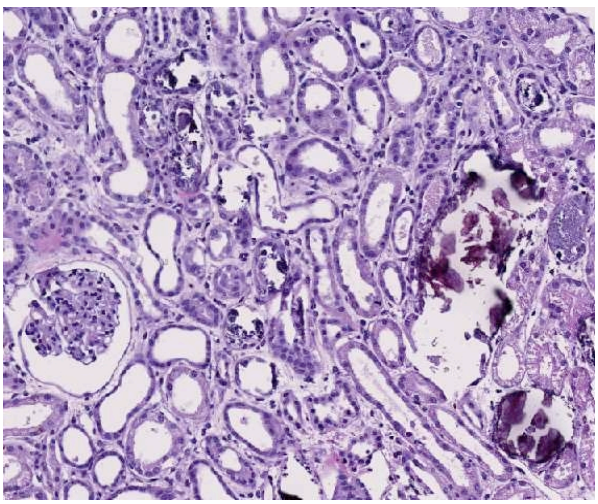

3-4. Kidney, dog: Diffusely, tubules are ectatic and lined by attenuated epithelium and often contains crystalline mineral. Bowman's space is also multifocally dilated. (HE 40X)

Contributor's Comment: A diagnosis of sub-acute ethylene glycol (EG) poisoning was confirmed by the detection of glycolic acid.

EG poisoning commonly occurs in dogs and cats after accidental ingestion of antifreeze solution. Cats are more susceptible than dogs, but dogs are more commonly affected.[3] EG is readily absorbed from the intestinal tract, but is in itself of low toxicity. While most EG is eliminated in the urine, some is metabolized by alcohol dehydrogenase to glycoaldehyde and its metabolites glycolic acid (GA), glyoxylate and oxalate. EG is rapidly metabolized while GA accumulates in plasma, and is detectable for a longer time period.[2] Glycoaldehyde and glyoxylate have been considered to be the primary nephrotoxic metabolites.[3] However, recent studies show that the calcium oxalate crystals might be most important for the renal toxicity.[4]

EG toxicity may progress through three stages. The first stage of EG toxicity is characterized by central nervous depression. The second stage is characterized by metabolic acidosis and is seen 12-24 hours after ingestion, and GA is the major contributor to this. The third stage includes oxalic acid excretion, nephropathy and eventual renal failure.[2,3]

Renal failure is due to toxic tubular necrosis and a renal edema that compromises the intrarenal blood flow. Tubular changes are most severe in proximal tubules and range from hydropic degeneration to necrosis to regeneration. The characteristic calcium oxalate crystals may be found in tubular lumina, in tubular cells and in the interstitium. While few calcium oxalate crystals may be seen in chronic tubular obstruction, large numbers of these crystals in renal tubules are virtually pathognomonic for EG poisoning.[3]

JPC Diagnosis: Kidney, proximal convoluted tubules: Degeneration and necrosis, diffuse, moderate, with abundant intratubular protein, mineral and numerous oxalate crystals, mild multifocal interstitial hemorrhage and edema.

Conference Comment: Conference participants discussed the diagnostic histopathologic findings and pathogenesis, as so well described by the contributor, in this example of a classic disease. In addition, participants considered the clinicopathologic findings associated with EG toxicity. The reported metabolic acidosis and hyperkalemia in this case correlate well with the diagnosis of EG toxicosis. A brief discussion of typical clinicopathologic findings in EG toxicosis follows.

Acid-base homeostasis is tightly regulated by major buffers such as hemoglobin and the bicarbonate buffer system as well as by minor buffers that include inorganic phosphate and plasma proteins.[5] The bicarbonate buffer system plays a major role in acid-base regulation and acts through the equilibrium reaction $H_2O + CO_2 \leftrightarrow H_2CO_3 \leftrightarrow H^+ + HCO_3^-$ to control the amount of hydrogen ions in (and thus the pH of) the blood.[1,5] The ratio of

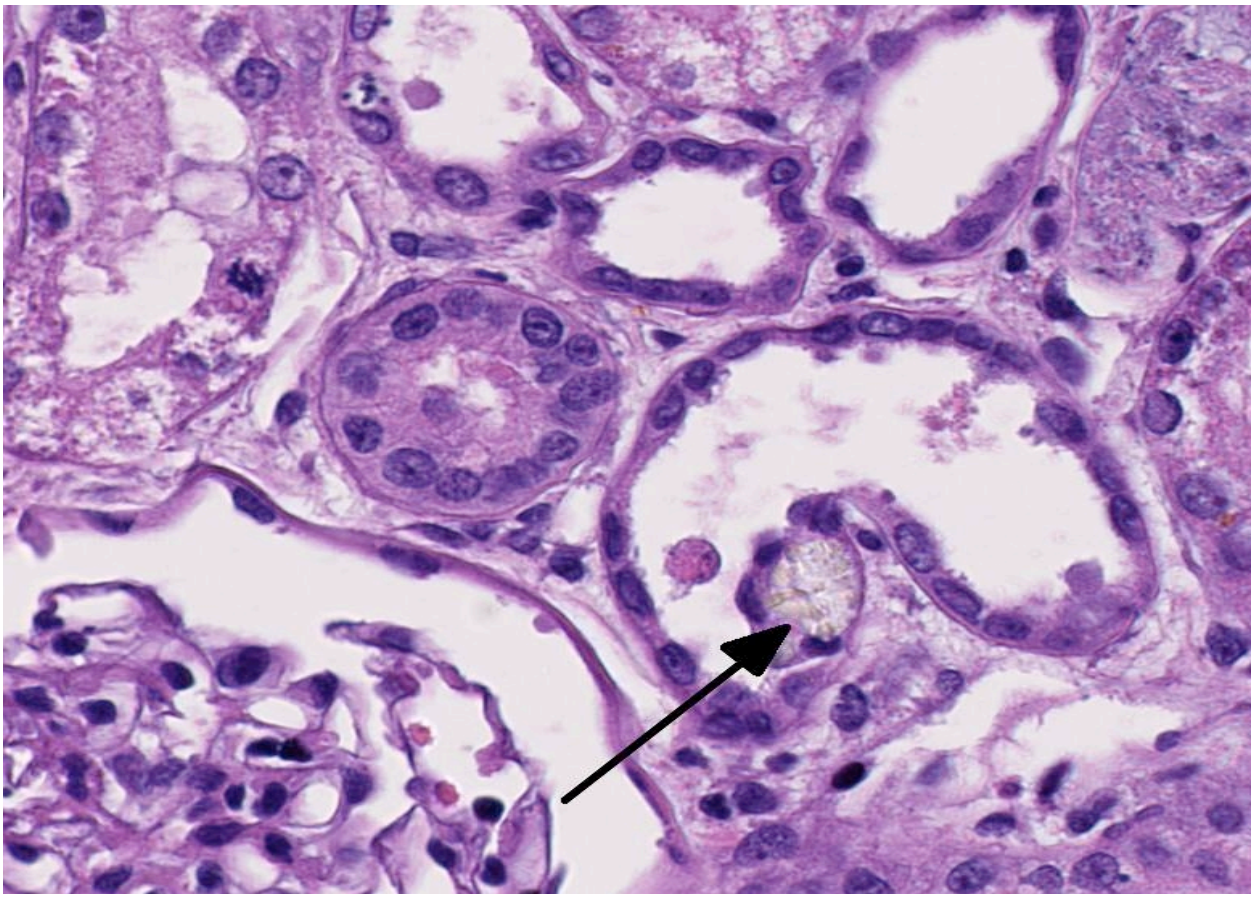

3-5. Kidney, dog: Occasionally, tubules contain an oval, fan- or prism-shaped birefringent oxalate crystal within the lumen (arrow). Additional changes such as necrosis (upper right), and regeneration (characterized by mitoseswithin epithelial cells at upper left) are present in this field. (HE 400X)

HCO_3^-/ H_2CO_3 determines the blood pH: An excess of acid (acidosis) leads to a decrease in blood pH (acidemia); whereas an excess of base (alkalosis) causes an increase in blood pH (alkalemia).[1] Disturbances in acid-base status are classified as either metabolic or respiratory, based on the underlying mechanism. Metabolic acidosis, the most common acid-base disturbance, is due to the production of acid by a pathologic metabolic processes.[5] Decreased plasma HCO_3^- (or serum TCO_2 concentrations, which is another way of measuring HCO_3^-) indicate metabolic acidosis.[1] In most species, plasma HCO_3^- or serum TCO_2 concentrations of 15 to 20 mmol/L is interpreted as moderate metabolic acidosis; whereas in the dog and cat, 12 to 17 mmol/L is consistent with moderate metabolic acidosis. Severe metabolic acidosis occurs when plasma HCO_3^- or serum TCO_2 concentrations are less than 15 mmol/L in most species and less than 12 mmol/L in the dog and cat.[1]

Common causes of metabolic acidosis include the following[1,5]:

- loss of bicarbonate (such as occurs with severe diarrhea, or decreased synthesis and loss of NaHCO3 by the renal tubules)
- excess in organic acids (titration acidosis)
    - lactic acidosis (from anaerobic glycolysis in hypoxia and shock; or excessive bacterial catabolism of carbohydrates)
    - ketoacidosis (acetoacetic acid and beta-hydroxybutyric acid in diabetic ketoacidosis, starvation or ketosis of ruminants)
    - renal failure (uremic acids)
    - acid toxicities (e.g. ethylene glycol toxicity)

As in this case, metabolic acidosis associated with EG toxicity is due to the EG metabolite, glycolic acid. Hyperkalemia, also as observed in this case, results from acidosis, as an excess of hydrogen ions causes a shift of potassium ions from intracellular to extracellular space. Additionally, oliguria in the

acute renal failure stage prevents excretion of potassium by the kidneys.[1]

In addition to these findings, EG toxicity is also often accompanied by a high anion gap, due to the presence of the salt of the organic acid.[1] Although not reported in this case, hypocalcemia is often observed in cases of EG toxicity; although renal disease can cause hypocalcaemia by a variety of mechanisms, in EG toxicosis, it is likely due to the sequestration of calcium in the formation of calcium oxalate crystals.[1]

Contributing Institution: Norwegian School of Veterinary Science
Departments of Basic Sciences and Aquatic Medicine
POB 8146 Dep N-0033
Oslo, Norway
www.nvh.no

References

1. George JW, Zabolotzky SM. Water, electrolytes, and acid base. In: Latimer KS, ed. *Duncan & Prasse's Veterinary Laboratory Medicine Clinical Pathology.* 5th ed. Ames, Iowa: Wiley-Blackwell; 2011:1145-171, 430.
2. Hess R, Bartels MJ, Pottenger LH. Ethylene glycol: an estimate of tolerable levels of exposure based on a review of animal and human data. *Arch Toxicol*. 2004;78:671-680.
3. Maxie M, Newman S. Urinary system. In:Maxie MG, ed. *Jubb, Kennedy & Palmer's Pathology of Domestic Animals*. Vol. 2. Edinburg, Scotland: Saunders Elsevier; 2007:425-522.
4. McMartin K. Are calcium oxalate crystals involved in the mechanism of acute renal failure in ethylene glycol poisoning? *Clin Toxicol*. 2009;47:859-869.
5. Weiser G. Laboratory of acid-base disorders. In: Thrall MA, Weiser G, Allison RW, Campbell TW, eds. *Veterinary Hematology and Clinical Chemistry.* Ames, Iowa: Wiley-Blackwell; 2012: Kindle edition, location *17216 of 37098.*

CASE IV: N1113774 (JPC 4022572).

Signalment: A 16-month-old male Sprague-Dawley rat (*Rattus norvegicus)*.

History: Shortly after arrival from the vendor, this aged male rat began T-maze training on a memory task to test cognitive loss with aging. Two weeks later the laboratory notified the veterinary staff of a mass on the ventral surface of the rat's neck. Physical examination of the ventral neck revealed, a 2 x 2 firm, non-mobile mass. A fine needle aspirate (FNA) collected from the mass consisted of neutrophils and macrophages. Two weeks treatment with oral enrofloxacin resulted in no change in the size of the mass; therefore, the rat was anesthetized for surgical excision of the mass. The right submandibular lymph node was removed with the mass. Excision was incomplete due to the location of the mass and approximation to the trachea, etc.
The biopsy revealed that the tumor was a high grade, poorly-differentiated adenocarcinoma and the rat was euthanized and submitted for necropsy.

Gross: Lung: There are numerous, multifocal, white, firm neoplastic masses encompassing approximately 50% of the lung lobes. Complete atelectasis of one lung lobe is observed and the distal surface of the right caudal lung lobe is adhered to the diaphragm.

Histopathologic Description: Submandibular salivary gland: The specimen consists of multiple lobules of submandibular salivary glands that are partially effaced and replaced by 2.5 cm unencapsulated irregular mass which extends into the surrounding soft tissues and to the limits of the section. The mass is comprised of irregular epithelial cells that infrequently form irregular ducts or acini. Density of tumor cells varies throughout the mass. Many anaplastic spindle-shaped tumor cells are also present. The neoplastic epithelial cells have marked nuclear pleomorphism, frequent prominent nucleoli and indistinct cell borders. Large foci of necrosis, scattered foci of hemorrhage and variable numbers of mitotic figures vary by field. Excision does not appear to be complete.

Review of a Masson's trichrome-stained section of tumor revealed that the neoplastic epithelial cells were negative for collagen while the desmoplastic tissue response was positive for collagen.

Morphologic Diagnosis: Submandibular salivary gland: Adenocarcinoma: high grade, poorly-differentiated.

Other significant microscopic findings (not submitted): Haired Skin, Incision Site of Tumor Removal: There are numerous small clusters to large foci (0.4 CM) of neoplastic cells similar in appearance to the primary tumor described in the biopsy report above scattered within the dermis and subcutis.

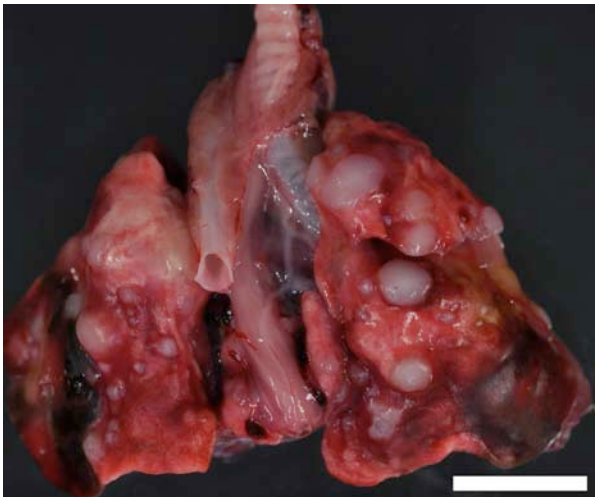

4-1. Lung: There are numerous, multifocal, white, firm neoplastic masses encompassing approximately 50% of the lung lobes. Complete atelectasis of one lung lobe is observed and the distal surface of the right caudal lung lobe is adhered to the diaphragm. (Photo courtesy of: The Section of Comparative Medicine Yale University School of Medicine, New Haven, CT)

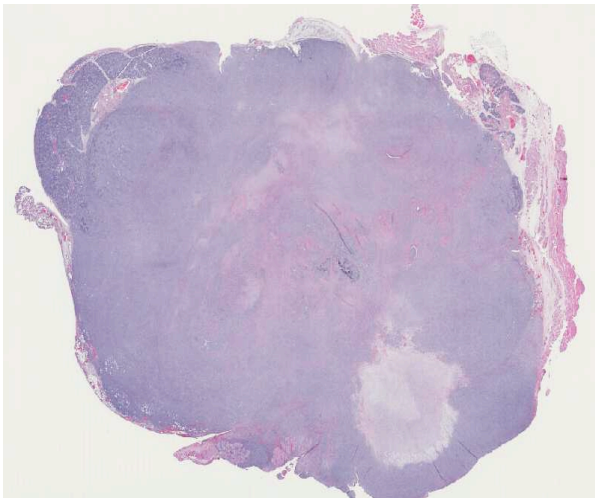

4-2. Submandibular salivary gland, rat: The submandibular salivary gland is effaced by a large neoplasm with multiple areas of necrosis. Normal salivary tissue is at upper left, with infiltration of skeletal muscle and adipose tissue around the rest of the periphery. (HE 0.63X)

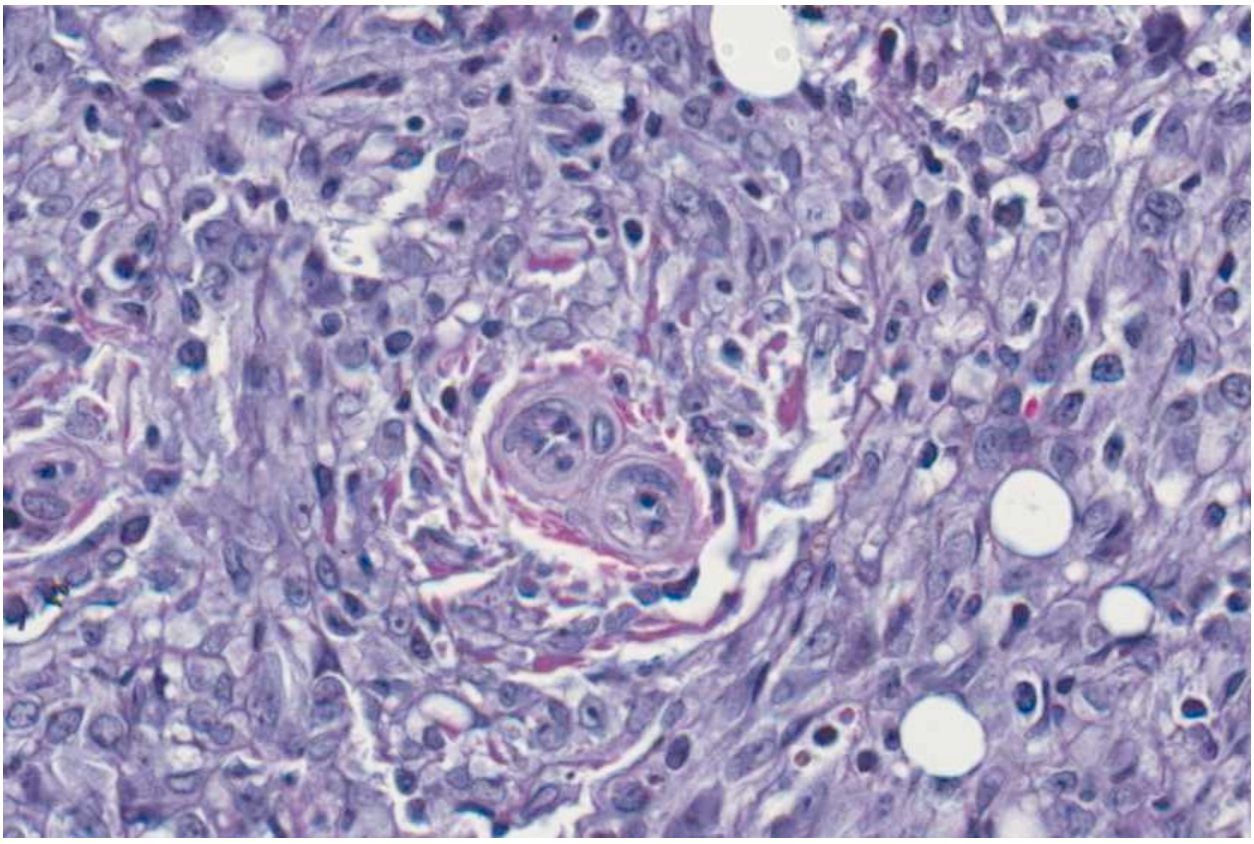

4-3. Submandibular salivary gland, rat: Neoplastic cells are spindle to polygonal with variably distinct cell border, eosinophilic to granular (zymogen) cytoplasm, and supported on a fine fibrovascular stroma in some area. Tumor cells appear to be forming acinar structures that have a clear lumen multifocally. (HE 400X)

Lung, Thymus (none visible): There is a metastatic neoplastic process admixed with hemorrhage and inflammation that effaces and replaces at least 50% of the lung. The neoplastic cells are similar in appearance to those described for the salivary gland mass above, with the exception of a greater epithelial cell component. Clusters and islands of neoplastic cells are frequent within alveoli. Hemorrhage, fibrin and inflammatory cells (macrophages) predominate within adjacent alveolar spaces.

Liver, Kidney, Adrenal Gland, Spleen, Pancreas: Within the one visible adrenal gland, 75% of the cortex and medulla are effaced and replaced by neoplastic cells similar in appearance to those described for the salivary gland above. There is bilateral mild to moderate chronic progressive glomerulonephropathy.

Contributor's Comment: Primary tumors of the major salivary glands are rare in humans, and the majority (>85%) are benign.[1,2,4,8,10,20,22,24] The incidence rate for both malignant and benign tumors is most common in patients between 50-70 years of age, but can occur at any age. There is also a wide geographic diversity of salivary gland tumor prevalence and frequency.[2,11,21] For example, it is reported that Canadian Eskimos have a greater prevalence (14/11,500/9years) of developing salivary gland carcinomas as compared to any other geographic group and they have a 100% mortality rate.[11] The majority of these tumors are undifferentiated lymphoepithelioma-like tumors found in mixed salivary glands.[21] Whereas in Denmark, they have a low prevalence of salivary gland carcinomas with an average of 1.1/100,000/ year and the most common type is a parotid gland carcinoma.[2]

Benign salivary gland tumors tend to occur more commonly in females, whereas malignant tumors are more prevalent in males.[10] Malignant salivary gland tumors can be diagnosed using the World Health Organization (WHO) classification system.[22] In general, mucoepidermoid carcinomas account for over 50% of malignant salivary gland tumors in humans, while adenocarcinomas were reported in

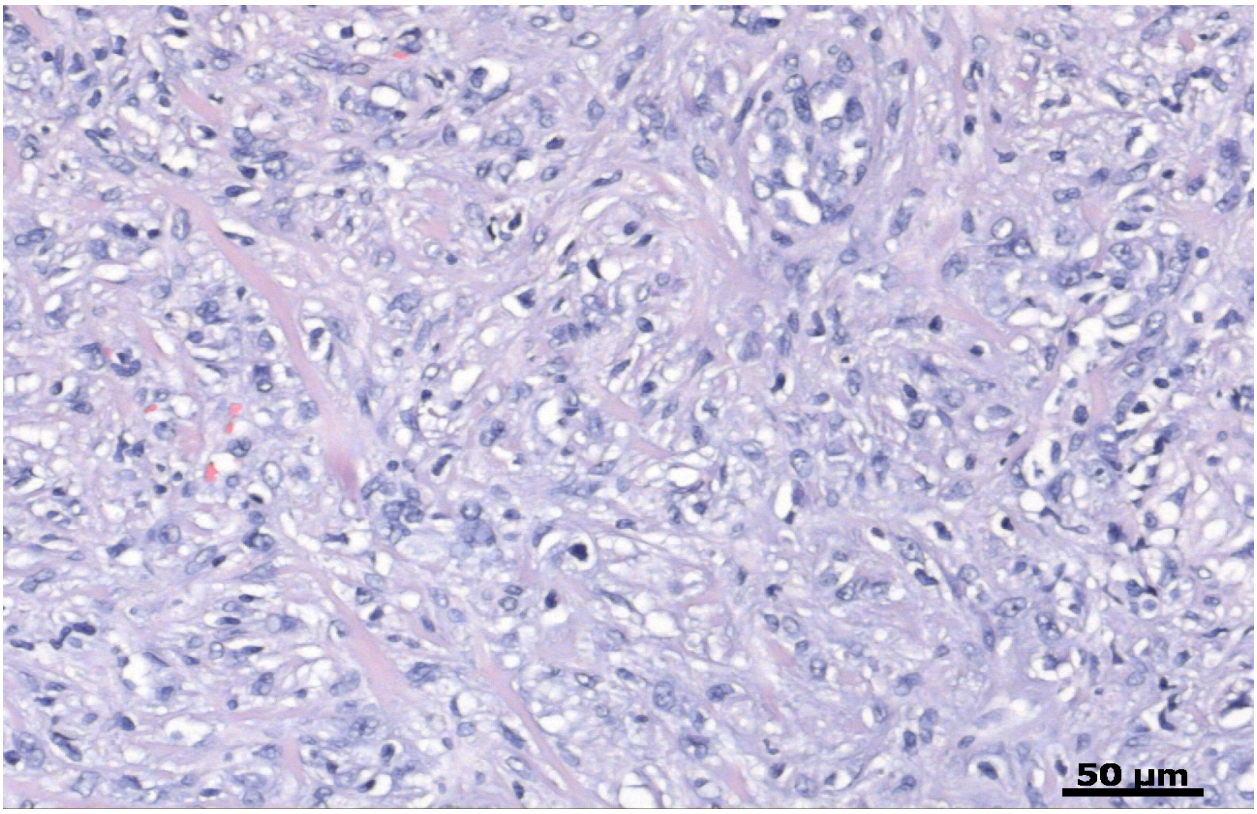

4-4. Submandibular salivary gland, rat: Within large areas of the neoplasm there are broad streams and bundles of spindle cells. Whether this population represents a phenotypic variation of a single population of neoplastic cells, or a second population within the neoplasm was a major source of discussion in this case. (Photo courtesy of: The Section of Comparative Medicine, Yale University School of Medicine, New Haven, CT)

only 12% of the cases. Tumors have been documented in all three major salivary glands, as well as in minor salivary glands; however, the most common site in humans is the parotid gland and the second most common being the submaxillary gland.[2,4,10,20,22]

In humans, submandibular gland tumors account for 5-15% of all salivary gland tumors and less than 1% of all malignant head and neck tumors, however, over 50% are malignant.[1] Malignant submandibular adenocarcinomas in humans tend to have areas of necrosis and hemorrhage with irregular and ill-defined margins that infiltrate growth into surrounding tissues. They tend to form nests or islands of tumor cells and have a widespread ductal differentiation. Clinically, over 20% of patients have reported pain and facial weakness associated with the mass.[14] Most tumors have progressed to high grade by the time they are diagnosed; therefore, these malignant submandibular salivary adenocarcinomas have a poor prognosis in humans.

Primary salivary gland tumors are also rare in domestic animals and have been reported in dogs[9,17], cats[13], lions[5], and cows.[3] In dogs, the most common salivary gland neoplasms are adenocarcinomas and carcinomas. There are two reports that describe rare cases in dogs, a malignant fibrous histiocytoma in a boxer[9] and another report of an osteosarcoma of the mandibular salivary gland in a collie.[17] Primary salivary gland tumors in cats are commonly carcinomas found in the minor salivary glands, rather than the parotid gland.[13] A single case of a high-grade mucoepidermoid carcinoma of the mandibular salivary gland has been reported in a lion.[5] There have also been three cases of parotid gland carcinomas reported in cows, two of which were pleomorphic carcinomas, and one was a squamous cell carcinoma.[3] Primary salivary gland tumors are also rare in rodents.[6,7,12,15,16,18,19,23] There has also been a single report of a Mongolian Gerbil developing a pleomorphic sarcoma of the salivary gland[18], and a ground squirrel with an adenocarcinoma of a minor salivary gland.[23] Mice very rarely develop salivary gland tumors, but myoepitheliomas have been reported to occur spontaneously in certain inbred strains of mice.

Spontaneous primary salivary gland tumors are also rare in rats, but may be chemically induced.[15,25] A

study during carcinogenesis in rat submandibular glands showed that histopathology and immunohistochemistry is a useful tool for tumor histiogenesis.[15] Submandibular salivary gland adenocarcinomas in rats are poorly differentiated, show local invasion, and, in most cases, incite a significant desmoplastic response.[7] They should also exhibit the same characteristics seen in human salivary glands, including nests or islands of tumor cells, and tumor-grade specific nuclear and mitoses characteristics. In this case, the rat demonstrated a significant amount of irregular epithelial cells, marked nuclear pleomorphism, prominent nucleoli, large area of necrosis, scattered foci of hemorrhage, a variable number of mitotic figures, with a desmoplastic tissue response. All of these characteristics are consistent with a diagnosis of a high grade submandibular salivary gland adenocarcinoma. Metastasis to the lungs and adrenal gland also indicates that this was a high-grade tumor with a poor prognosis.

JPC Diagnosis: Submandibular salivary gland: Carcinoma, poorly-differentiated.

Conference Comment: The contributor does an excellent job of summarizing salivary gland tumors in humans and animals. We agree that this neoplasm is both a high grade malignancy and poorly-differentiated; however, we prefer a more general diagnosis of poorly-differentiated salivary gland carcinoma. In this case, we considered diagnoses of salivary gland adenocarcinoma and myoepithelial carcinoma, as conference participants discussed whether or not the spindle cells represent either a desmoplastic response to tumor invasion or perhaps, a neoplastic component in itself. Immunophenotyping of the spindle cell population revealed a diffuse, strong cytoplasmic immunoreactivity for vimentin and scattered cytoplasmic immunoreactivity for both smooth muscle actin and calponin, (a myoepithelial cell marker). In addition to the poorly-differentiated tumor cell morphology, additional features of malignancy include local invasion into the surrounding adipose and skeletal muscle, areas of necrosis and neoplastic thrombi within blood vessels. Also present and of descriptive interest are individual and clusters of mast cells within the neoplasm, as well as ductal hyperplasia within the preexisting, entrapped salivary gland.

Contributing Institution: Section of Comparative Medicine
Yale University School of Medicine
New Haven, CT

References:

1. Bhattacharyya N. Survival and prognosis for cancer of the submandibular gland. *J Oral Maxillofac Surg*. 2004;62:427-430.
2. Bjorndal K, Krogdahl A, Therkildsen MH, Overgaard J, Johansen J, Kristensen CA, et al. Salivary gland carcinoma in Denmark 1990-2005: a national study of incidence, site and histology. Results of the Danish Head and Neck Cancer Group (DAHANCA). *Oral Oncol*. 2011;(47):677-682.
3. Bundza A. Primary salivary gland neoplasia in three cows. *J Comp Pathol*. 1983;93:629-632.
4. Cho KJ, Ro JY, Choi J, Choi SH, Nam SY, Kim SY. Mesenchymal neoplasms of the major salivary glands: clinicopathological features of 18 cases. *Eur Arch Otorhinolaryngol*. 2008;(265 Suppl 1): S47-56.
5. Dorso L, Risi E, Triau S, Labrut S, Nguyen F, et al. High-grade mucoepidermoid carcinoma of the mandibular salivary gland in a lion (Panthera leo). *Vet Pathol*. 2008;45:104-108.
6. Ishikawa Y, Nishimori K, Tanaka K, Kadota K. Naturally occurring mucoepidermoid carcinoma in the submandibular salivary gland of two mice. *J Comp Pathol*. 1998;118:145-149.
7. Nishikawa S, Sano F, Takagi K, Okada M, Sugimoto J, Takagi S. Spontaneous poorly differentiated carcinoma with cells positive for vimentin in a salivary gland of a young rat. *Toxicol Pathol*. 2010;38:315-318.
8. Pang B, Leong CC, Salto-Tellez M, Petersson F. Desmoplastic small round cell tumor of major salivary glands: report of 1 case and a review of the literature. *Appl Immunohistochem Mol Morphol*. 2011;19:70-75.
9. Perez-Martinez C, Garcia Fernandez RA, Reyes Avila LE, Perez-Perez V, Gonzalez N, Garcia-Iglesias MJ. Malignant fibrous histiocytoma (giant cell type) associated with a malignant mixed tumor in the salivary gland of a dog. *Vet Pathol*. 2000;37:350-353.
10. Pinkston JA, Cole P. Incidence rates of salivary gland tumors: results from a population-based study. *Otolaryngol Head Neck Surg*. 1999;120:834-840.
11. Schaefer O, Hildes JA, Medd LM, Cameron DG. The changing pattern of neoplastic disease in Canadian Eskimos. *Can Med Assoc J*. 1975;112:1399-1404.
12. Slavin BG, Paule WJ, Bernick S. Morphological changes in the submandibular gland of aging rats. *Gerodontology*. 1989;8:53-58.

13. Sozmen M, Brown PJ, Eveson JW. Salivary duct carcinoma in five cats. *J Comp Pathol*. 1999;121:311-319.
14. Spiro RH, Huvos AG, Strong EW. Adenocarcinoma of salivary origin. Clinicopathologic study of 204 patients. *Am J Surg*. 1982;144:423-431.
15. Sumitomo S, Hashimura K, Mori M. Growth pattern of experimental squamous cell carcinoma in rat submandibular glands--an immunohistochemical evaluation. *Eur J Cancer B Oral Oncol*. 1996;32B: 97-105.
16. Sundberg JP, Hanson CA, Roop DR, Brown KS, Bedigian HG. Myoepitheliomas in inbred laboratory mice. *Vet Pathol*. 1991;28:313-323.
17. Thomsen BV, Myers RK. Extraskeletal osteosarcoma of the mandibular salivary gland in a dog. *Vet Pathol*. 1999;36:71-73.
18. Toyoda T, Tsukamoto T, Cho YM, Onami S, Takasu S, Shi L, et al. Undifferentiated sarcoma of the salivary gland in a Mongolian gerbil (Meriones unguiculatus). *J Toxicol Pathol*. 2011;24:173-177.
19. Tsunenari I, Yamate J, Sakuma S. Poorly differentiated carcinoma of the parotid gland in a six-week-old Sprague-Dawley rat. *Toxicol Pathol*. 1997;25:225-228.
20. Vargas PA, Gerhard R, Araujo Filho VJ, de Castro IV. Salivary gland tumors in a Brazilian population: a retrospective study of 124 cases. *Rev Hosp Clin Fac Med Sao Paulo*. 2002;57:271-276.
21. Wallace AC, Macdougall JT, Hildes JA, Lederman JM. Salivary gland tumors in Canadian Eskimos. *Cancer*. 1963;16:1338-1353.
22. Barnes L. Tumors of the salivary glands. In: Barnes L, Eveson JW, Reichart P, Sidransky D, eds. *World Health Organization (WHO): The WHO Classification of Head and Neck Tumours*. *Pathology and Genetics of Head and Neck Tumours*. Lyon, France: International Agency for Research on Cancer (IARC) Press. 2005:209-281.
23. Yamate J, Yamamoto E, Nabe M, Kuwamura M, Fujita D, Sasai H. Spontaneous adenocarcinoma immunoreactive to cyclooxygenase-2 and transforming growth factor-beta1 in the buccal salivary gland of a Richardson's ground squirrel (Spermophilus richardsonii). *Exp Anim*. 2007;56:379-384.
24. Yin WH, Guo SP, Yang HY, Chan JK. Desmoplastic small round cell tumor of the submandibular gland--a rare but distinctive primary salivary gland neoplasm. *Hum Pathol*. 2010;41:438-442.
25. Zaman A, Kohgo T, Shindoh M, Iizuka T, Amemiya A. Induction of adenocarcinomas in the submandibular salivary glands of female Wistar rats treated with 7,12-dimethylbenz(a)anthracene. *Arch Oral Biol*. 1996;41:221-224.